Oncogene (2020) 39:739–753
https://doi.org/10.1038/s41388-019-1024-y

ARTICLE

Bone-marrow-derived cell-released extracellular vesicle miR-92a regulates hepatic pre-metastatic niche in lung cancer

Ya-Ling Hsu[1] · Ming-Shyan Huang[2,3] · Jen-Yu Hung[4,5] · Wei-An Chang[4,5,6] · Ying-Ming Tsai[1,4,5] · Yi-Chung Pan[6] · Yi-Shiuan Lin[6] · Hung-Pei Tsai[7] · Po-Lin Kuo[6,8,9]

Received: 3 January 2019 / Revised: 29 April 2019 / Accepted: 11 May 2019 / Published online: 26 September 2019

Abstract

Metastatic tumors have been shown to establish a supportive pre-metastatic niche (PMN) in distant organs, which in turn determines disseminated tumor cells' targeting of such organs. PMN is formed through the recruitment of bone-marrow-derived cells (BMDCs); however, the role of BMDCs in PMN formation is not fully understood. On the basis of RNA-seq data and bioinformatic analysis, secretion of extracellular vesicle (EV) miR-92a by BMDCs of lung cancer-bearing mice contributes to the establishment of liver PMN. Both BMDC-derived EVs and miR-92a mimics potentiate the activation of hepatic stellate cells (HSCs), subsequently increasing extracellular matrix (ECM) deposition in mice. Consequently, remodeling of the liver microenvironment enhanced immunosuppressive cell accumulation and cancer cell attachment. EVs miR-92a directly suppressed its target *SMAD7*, leading to the enhancement of transforming growth factor-β signaling in HSC. Elevated levels of circulating miR-92a are found in the sera of lung cancer patients, and EVs isolated from these patients have a similar ability to increase HSCs activation and ECM protein expression. Our study reveals the sequential steps of liver PMN formation in lung cancer, providing critical mediators that prepare PMN in the liver, and identifies new targets that offer valuable options for diagnosis and therapeutic intervention.

Supplementary information The online version of this article (https://doi.org/10.1038/s41388-019-1024-y) contains supplementary material, which is available to authorized users.

✉ Po-Lin Kuo
kuopolin@seed.net.tw

1 Graduate Institute of Medicine, College of Medicine, Kaohsiung Medical University, 807 Kaohsiung, Taiwan

2 Department of Internal Medicine, E-DA Cancer Hospital, 840 Kaohsiung, Taiwan

3 School of Medicine, I-Shou University, 840 Kaohsiung, Taiwan

4 Division of Pulmonary and Critical Care Medicine, Kaohsiung Medical University Hospital, 807 Kaohsiung, Taiwan

5 School of Medicine, College of Medicine, Kaohsiung Medical University, 807 Kaohsiung, Taiwan

6 Graduate Institute of Clinical Medicine, College of Medicine, Kaohsiung Medical University, 807 Kaohsiung, Taiwan

7 Division of Neurosurgery, Department of Surgery, Kaohsiung Medical University Hospital, 807 Kaohsiung, Taiwan

8 Center for Cancer Research, Kaohsiung Medical University, 807 Kaohsiung, Taiwan

9 Institute of Medical Science and Technology, National Sun Yat-Sen University, 804 Kaohsiung, Taiwan

Introduction

Lung cancer is the most common malignancy, and causes the highest number of cancer-related deaths worldwide [1]. Metastasis is common in lung cancer, and the average 5-year survival rate of patients with metastasized lung cancer is only ~15% [2, 3]. Lung cancer metastasizes to many organs, including the adrenal glands, bones, brain, and liver, each of which requires different shaping in the environment of destination for the adaptation of arriving cancer cells to foreign environments [4]. Organ-specific metastasis is dependent on the formation of pre-metastatic niches (PMN), which includes angiogenesis, extracellular cellular matrix (ECM) remodeling, and aberrant immune cell accumulation [5, 6]. Improved understanding of the formation of PMN during the metastatic process is clearly needed, so that promising new therapeutic strategies can be developed to prevent and treat metastatic cancer.

Liver metastases will develop in 20–30% of non-small cell lung cancer patients, and is a significant factor in poor prognoses [7]. Hepatic stellate cells (HSCs) are postulated as the most important cellular component in liver pre-metastatic niche, because they can transdifferentiate to an

activated status implicated in the alteration of the ECM and suppressive immune cells' recruitment [8, 9]. The phenotypic changes of active HSCs include expression of α-smooth muscle actin (α-SMA), a high degree of proliferation, and elevated ECM deposits [10]. Active HSC promotes incoming cancer cell survival and growth in the liver environment by supplying cancer cells with growth factors and cytokines, regulating ECM turnover, and suppressing immune response [11]. The immunosuppressive environment constructed by HSC is achieved by a myeloid-derived suppressor cell (MDSC) population, which consists of heterogeneous cells that can be divided into two subgroups with distinct phenotypes: granulocytic ($Cd11b^{+}Ly6G^{+}Ly6C^{low}$, gMDSC) and monocytic ($CD11b^{+}Ly6G^{-}Ly6C^{hi}$, mMDSC) cells [11, 12]. To date, cancer cells are the only cellular regulator hypothesized to activate HSCs by secreting transforming growth factor-beta (TGF-β). However, multiple cells and complex genetic mechanisms have been demonstrated to play a part in the regulation of HSC activation in liver-related disease [13]. Therefore, the activation of quiescent HSC by cancer still requires future investigation.

Malignancy is considered a systemic disorder because it can alter and respond to the whole body environment via multifaceted communications to facilitate disease progression [14, 15]. Bone marrow and bone-marrow-derived cells (BMDC) is a tissue of particular concern, due to its containing abundant types of progenitors, which control hematopoiesis and immune cell fate [16, 17]. Cell-shed membrane vesicles, carrying various signaling molecules secreted and internalized by different cell types, are widely accepted as participating in distant cell-cell communication [18, 19]. A recent study reveals that lung cancer remotely affects osteocalcin expressing cells residing in bone marrow, which create favorable tumor microenvironments and facilitate cancer progression [15]. Extracellular vehicles (EVs) have been known to be involved in the establishment of metastatic organotropism by systemic interaction, resulting in an increase of metastatic burden [9]. In this study, we set out to identify the BMDCs that promote the liver-specific metastasis of lung cancer, and to investigate the underlying mechanisms. Our study has revealed that BMDC-secreted EVs miR-92a specifically promotes lung cancer metastasis to the liver by increasing the activation of HSC, as well as subsequent ECM remodeling and gMDSC accumulation in the liver. Specifically, we show that BMDC-secreted EV miR-92a enhances the aforementioned processes by enabling lung cancer cells to (1) potentiate the effect of TGF-β on HSC activation by overcoming the inhibitory effect of SMAD7, (2) create a favorable immune-suppressive microenvironment in the liver, and (3) exploit constituents for the cancer colonization signals produced by HSC in the liver. Our study reveals that BMDC-secreted EVs are essential for formation of liver PMN, and could potentially be a therapeutic in targeting lung cancer.

Results

The alteration of liver microenvironments and BMDCs in mice with lung cancer

To investigate whether the liver microenvironment is changed in lung cancer-bearing mice prior to cancer metastasis, we assessed several characteristics of liver PMN, including HSC activation, ECM protein (vitronectin, tenascin C, collagen type I, and fibronectin) upregulation and recruitment of MDSCs in livers of Lewis lung carcinoma (LLC)-bearing mice (Fig. 1a). IHC results reveal that, compared to the livers of normal mice, both HSC activation (increased α-SMA) and collagen type I increase in the livers of LLC-bearing mice, but not vitronectin, tenascin C, and fibronectin. (Fig. 1b). In addition, the cell population of gMDSC, but not mMDSC, increases 2.94-folds in the livers of LLC-bearing mice, when compared to normal mice (Fig. 1c, d). Consistent with these results, the HSC activation and collagen type I upregulation are also found in the liver in human lung H460 cancer-bearing mice. The gMDSC accumulation, increased in the livers of H460-bearing mice, although the difference between two groups did not reach statistical significance (Supplementary Fig. 1A, 1B)

To assess whether the gene profile of BMDCs changes in lung cancer-bearing mice, and may therefore be involved in the formation of metastatic niches in distant organs, we compared miRNA expressions of BMDCs of normal and LLC-bearing mice. Next-generation sequencing (NGS) data reveal that 106 miRNAs were upregulated in BMDCs of LLC-bearing mice (Fig. 1e). We evaluated the specific functional categories of upregulated miRNAs using Ingenuity Pathway Analysis (IPA). The results indicated that the top 6 ranked Biological Functions and Disease categories are cancer, connective discords, organismal injury and abnormalities, reproductive system disease, immunological disease, and inflammatory disease. In addition, the top 6 ranked Pathway and Tox list are renal inflammation, renal nephritis, cardiac fibrosis, hepatocellular carcinoma, and liver hyperplasia/hyperproliferation categories (Fig. 1f and Table 1). These results suggested that BMDC may be involved in the formation of liver PMN.

Changes in liver microenvironments promote metastasis of lung cancer

Next, we determined whether changes of the liver niche due to HSC activation promote lung cancer metastasis to the liver. The attachment ability of lung cancer was evaluated in

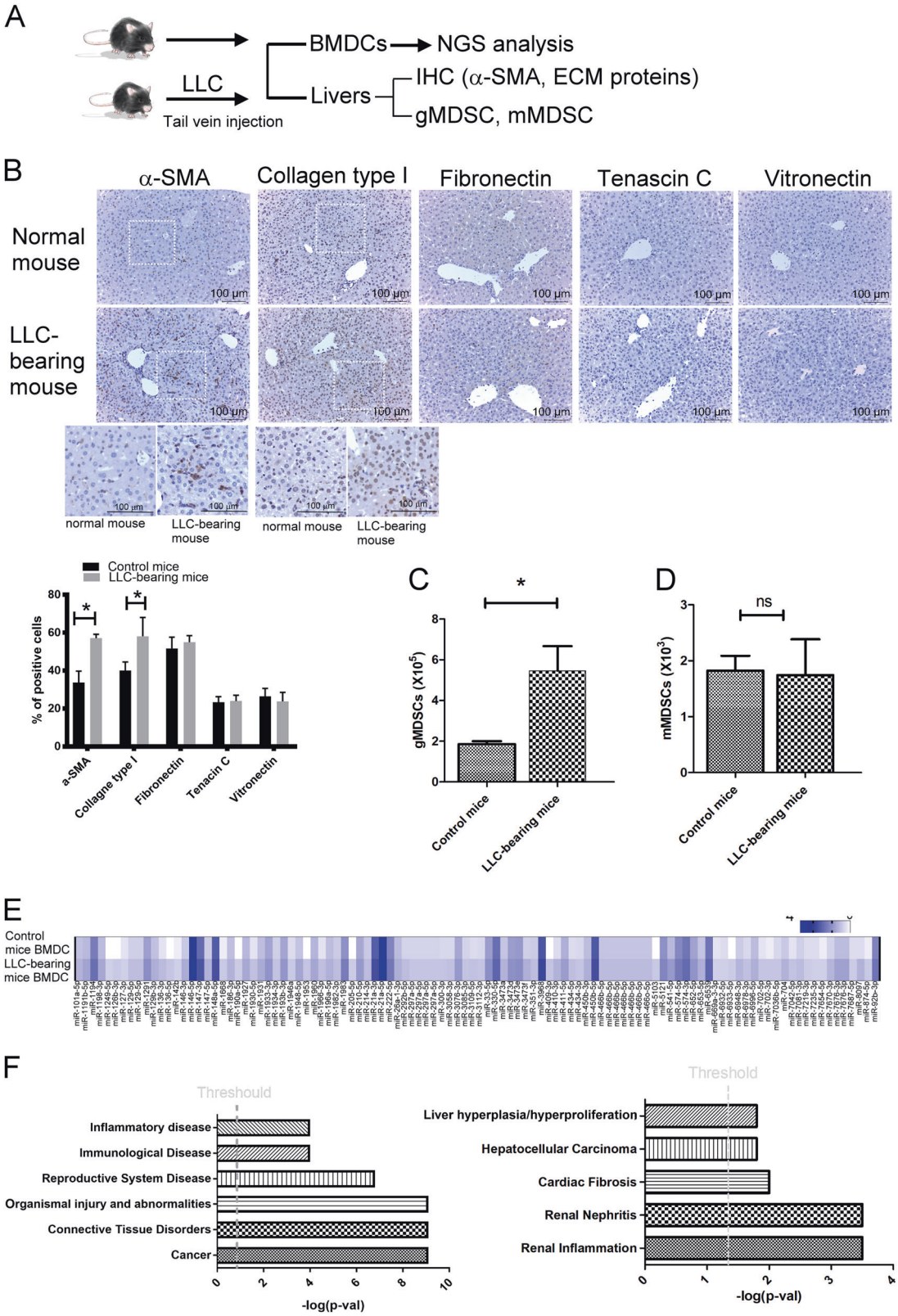

mouse HSC (mHSC) activated by TGF-β stimulation. TGF-β induced the activation of mHSC, and increased the expression of collagen type I (Supplementary Fig. 2A, 2B). Activated mHSC not only increased the adhering of LLC, but also enhanced the transendothelial migration of gMDSC isolated from LLC-bearing mice (Supplementary Fig. 2C,

◀ **Fig. 1** The changes of liver niche and bone-marrow-derived cells (BMDCs) in LLC-bearing mice. **a** Scheme of the animal models. The alterations of HSC activation and ECM proteins (**b**), and the accumulation of gMDSC (**c**) and mMDSC cells (**d**) of livers in LLC-bearing mice. (**e**) miRNA profile and (**f**) IPA analysis of BMDCs miRNAs. LLC was implanted into mice by tail vein injection. After 10 days, the BMDCs were collected and miRNA expressions assessed by NGS and IPA. The livers of mice were harvested and stained using the indicated antibodies. gMDSC and mMDSC cells were isolated from the livers of normal mice and LLC-bearing mice. The livers of these mice were harvested and stained with IHC. Digital images of tissues were captured and analyzed with ImageJ software to calculate the percentage of positive cells (high-positive + positive + low-positive cells). Each value is the mean ± SEM; *Significant difference between the two test groups, as analyzed by Student's *t*-test ($p < 0.05$), ns, not significant, α-SMA smooth muscle actin, BMDC bone-marrow-derived cells, ECM extracellular matrix, LLC Lewis lung carcinoma, gMDSC granulocytic myeloid-derived suppressor cell, mMDSC monocytic MDSC

2D). To assess whether these changes increase liver metastasis of lung cancer in vivo, we secondarily implanted LLC via splenic injection in mice with or without LLC (Supplementary Fig. 2E). Supplementary Fig. 2E, 2F shows that the ratio of liver metastasis increased in the LLC mice after the secondary implantation. These data suggest lung cancer could shape a PMN in the liver prior to the spread of cancer.

BMDCs are involved in the formation of PMN in liver

EVs are implicated as being critical signalosomes in the long-distance cross-talk between various cell types [18, 19]. Consequently, we collected EVs of BMDCs isolated from normal and LLC-bearing mice and evaluated their effect in HSC activation. We isolated and characterized EVs from BMDCs using transmission electron microscopy (TEM) and immunoblot (using CD63, CD81, TSG101, CD9, and HSP70 as exosome markers). Nanovesicles with a size of ≤200 nm were found in EVs of BMDCs (Fig. 2a). EVs markers, including CD63, CD81, TSG101, CD9, HSP70, and acetecylcholinesterase were also observed in EVs isolated from BMDCs (Fig. 2b, c). mHSC exhibited an efficient uptake of EVs, as indicated by the internalization of Dil-labelled BMDC-EVs (Fig. 2d). Compared to the EVs obtained from BMDCs of normal mice, EVs isolated from the BMDCs of LLC-bearing mice increased mHSC activation, collagen type I expression and LLC attachment (Fig. 2e, g). Treatment of mice with EVs isolated from the BMDCs of LLC-bearing mice by retro-orbital injection increased HSC activation and collagen type I deposition in liver in vivo (Fig. 2h). Moreover, pretreated mice with EVs isolated from the BMDCs of LLC-bearing mice also revealed enhanced liver metastasis of LLCs (Fig. 2i–k). These results show that BMDCs contribute to the liver's PMN formation, and subsequently, liver metastasis of lung cancer via EVs delivery.

BMDCs increased HSC activation and collagen type I expression by EVs miR-92a

To identify BMDC EV-associated small RNAs, we measured the levels of EVs miRNAs which were upregulated in the BMDCs of LLC-bearing mice, and predicated to be a regulator by IPA for liver hyperplasia/hyperproliferation (Table 1). qRT-PCR results show that the miR-92 family (miR-92a and miR-92b have the same seed region to target 3'UTR of mRNA) was enhanced in the BMDC-derived EVs of LLC-bearing mice (Fig. 3a and Supplementary Fig. 3A). Because the levels of miR-92a were higher than miR-92b in both BMDCs and their secretory EV (RPM (Reads per million) of NGS: 6858.44 vs. 29.44 in EVs of LLC mouse BMDCs and 4396.43 vs. 75.6 in EVs of normal mouse BMDCs), we suggest that miR-92a, but not miR-92b contributes to the shaping of liver PMN. The elevated miR-92a is also found in the EVs isolated from BMDCs of H460-bearing mice (Supplementary Fig. 3B). mHSC which received EVs isolated from LLC-bearing mice presented higher levels of mature miR-92a, but not pre-miR-92a and miR-92b when compared to mHSC which had received EVs isolated from the BMDCs of LLC-bearing mice (Fig. 3b, Supplementary Fig. 3C, D). Moreover, inhibition of miR-92a prevented the effects of BMDC-derived EVs in HSC activation and collagen type I expression, supporting the hypothesis that miR-92a is involved in the formation of liver PMN in lung cancer (Fig. 3d, e).

We also assessed the effects of miR-92a on HSC activation and collagen type I expression using human HSC (hHSC) LX2 cells. Transfection of miR-92a mimics increased the effects of TGF-β in the upregulation of α-SMA and collagen type I expression in both LX2 cells and mHSCs (Fig. 3f, g). In addition, transfection of miR-92a mimics to HSCs also enhances the attachment of lung cancer cell lines H1299 and LLC on LX2 cells and mHSC, respectively (Fig. 3h).

miR-92a increased the activation of HSCs induced via TGF-β by targeting SMAD7

We performed experiments to determine possible miR-92a targets that may contribute to regulating activity in HSC activation by using three predicted miRNAs websites, including Targetscan, MiRanda and Pictar. In silico analysis predicted a single, species-conserved miR-92a binding site in the 3′UTRs of SMAD7, which belongs to inhibitory SMAD7 (Fig. 4a). 3′ untranslated region (3'UTR) luciferase reporter analysis has shown that miR-92a mimics exhibit a direct binding on wild-type 3'UTR of SMAD7, but not on mutated 3′UTR luciferase plasmid (Fig. 4b). Consistent with the 3'UTR luciferase reporter analysis, miR-92a mimics decreased the expression of SMAD7 and

Table 1 The miRNAs are predicted to involve in cancer, connective tissue disorders, organismal injury and abnormalities, and liver-related disease

Molecules	Categories	*p*-Value	Upregulation (folds) by NGS
miR-127-3p	Cancer, connective tissue disorders, organismal injury and abnormalities	7.43E-10	2.833333
miR-128-3p	Cancer, organismal injury and abnormalities, reproductive system disease	1.49E-07	2.044872
miR-129-5p	Cancer, organismal injury and abnormalities, reproductive system disease	8.05E-07	2.595238
miR-196a-5p	Cancer, gastrointestinal disease, organismal injury and abnormalities, respiratory disease	1.64E-04	2.094444
miR-146a-5p	Cancer, organismal injury and abnormalities, hepatocellular carcinoma, liver hyperplasia/hyperproliferation	7.03E-05	4.296296
miR-204-5p	Cancer, gastrointestinal disease, organismal injury and abnormalities	9.85E-04	4.25
miR-330-5p	Cancer, gastrointestinal disease, organismal injury and abnormalities	2.30E-03	2.018203
miR-21-5p	Cancer, organismal injury and abnormalities, respiratory disease	4.28E-03	3.001535
miR-92b-3p	Cancer, organismal injury and abnormalities, liver hyperplasia/hyperproliferation	2.54E-02	2.567935
miR-193a-3p	Cancer, organismal injury and abnormalities, renal and urological disease	2.88E-02	2.538767
miR-92a-3p	Cancer, organismal injury and abnormalities, renal and urological disease	2.54E-02	1.56

increased SMAD2 phosphorylation in LX2 cells after TGF-β stimulation (Fig. 4c). Stable overexpression of SMAD7 prevents the enhanced effect of miR-92a on TGF-β-mediated SMAD2 phosphorylation, HSC activation and collagen type I expression (Fig. 4d–f). Moreover, the effects of miR-92a mimics on the enhancement of lung cancer H1299 cells attaching to hHSC were also prevented by SMAD7 overexpression (Fig. 4g).

To determine which type of BDMCs is the major source of miR-92a, we assessed levels of miR-92a in the EVs secreted by hematopoietic progenitor cells (HPC), MDSCs, CD11c+ and CD11b+ cells in LLC-bearing mice. The results show that level of miR-92a in CD11b+ cell-derived EVs of LLC-bearing mice was higher than that of EVs derived by CD11b+ cell-derived EVs of normal mice (Supplementary Fig. 4A). In contrast, the level of EVs miR-92a were not significantly different between HPC, CD11c + cells and MDSCs (monocytic and gMDSC) isolated from normal and LLC-bearing mice (Supplementary Fig. 4B, E). These data show that CD11b+ cells of BMDCs are involved in the formation of liver PMN.

miR-92a mimics increase liver metastasis in mice

To address whether miR-92a may increase liver metastasis in vivo, miR-92a mimics were administered by retro-orbital injection for 3 weeks, then LLC cells were implanted in the mice via splenic injection (Fig. 5a). To confirm the efficacy and toxicity of miR-92a delivery, we assessed the levels of miR-92a in several organs, together with blood cell counts and biochemical parameters. Compared to control mimics' delivery, miR-92a mimics had higher levels in liver by retro-orbital *injection*, but not in lungs, kidneys, spleens, and heart (Supplementary Fig. 5A). No significant changes were observed in the biochemical markers for liver, kidneys and bone marrow functions (sTable 1). As a parameter of tissue damage, organ weight was also measured but showed no difference between the control mimics and miR-92a-treated groups (Supplementary Fig. 5B). No histological abnormalities in the liver, lungs, and kidneys were detected (Supplementary Fig. 5C). All inflammatory cytokines of liver were also no difference between the control mimics and miR-92a-treated groups (Supplementary Fig. 5D). These data show retro-orbital injection effectively delivers miR-92a mimics to the livers without significant toxicity. In contrast, miR-92a mimics enhanced HSC activation and collagen type I expression in the livers of mice (Fig. 5b). In addition, miR-92a mimics also increased the tumor's capacity to metastasize to the liver. The liver nodules of mice, which had been administered miR-92a mimics displayed more and larger of tumors, as well as local invasion around the tumors (Fig. 5c, d). Next, we assessed whether targeting miR-92a decreased pre-metastatic niche formation in the liver. EVs isolated from BMDC of normal or LLC-bearing mice and the miR-92a inhibitors were administered by retro-orbital injection for 3 weeks, then LLC cells were implanted via splenic injection. The results indicate that miR-92a inhibitor not only decreases HSC activation and collagen type I expression the livers, but also reduces liver metastasis of mouse lung cancer LLC (Fig. 5e–g).

Elevated levels of EV miR-92a are found in lung cancer patients' sera

To further elucidate the nature of the EV miR-92a present in the sera of lung cancer patients, we compared serum EV miR-92a levels among healthy donors ($n = 18$) and lung cancer patients ($n = 19$). Circulating EVs purified from sera and miR-92a levels were measured by real-time polymerase chain reaction. Compared to healthy donors, miR-92a levels

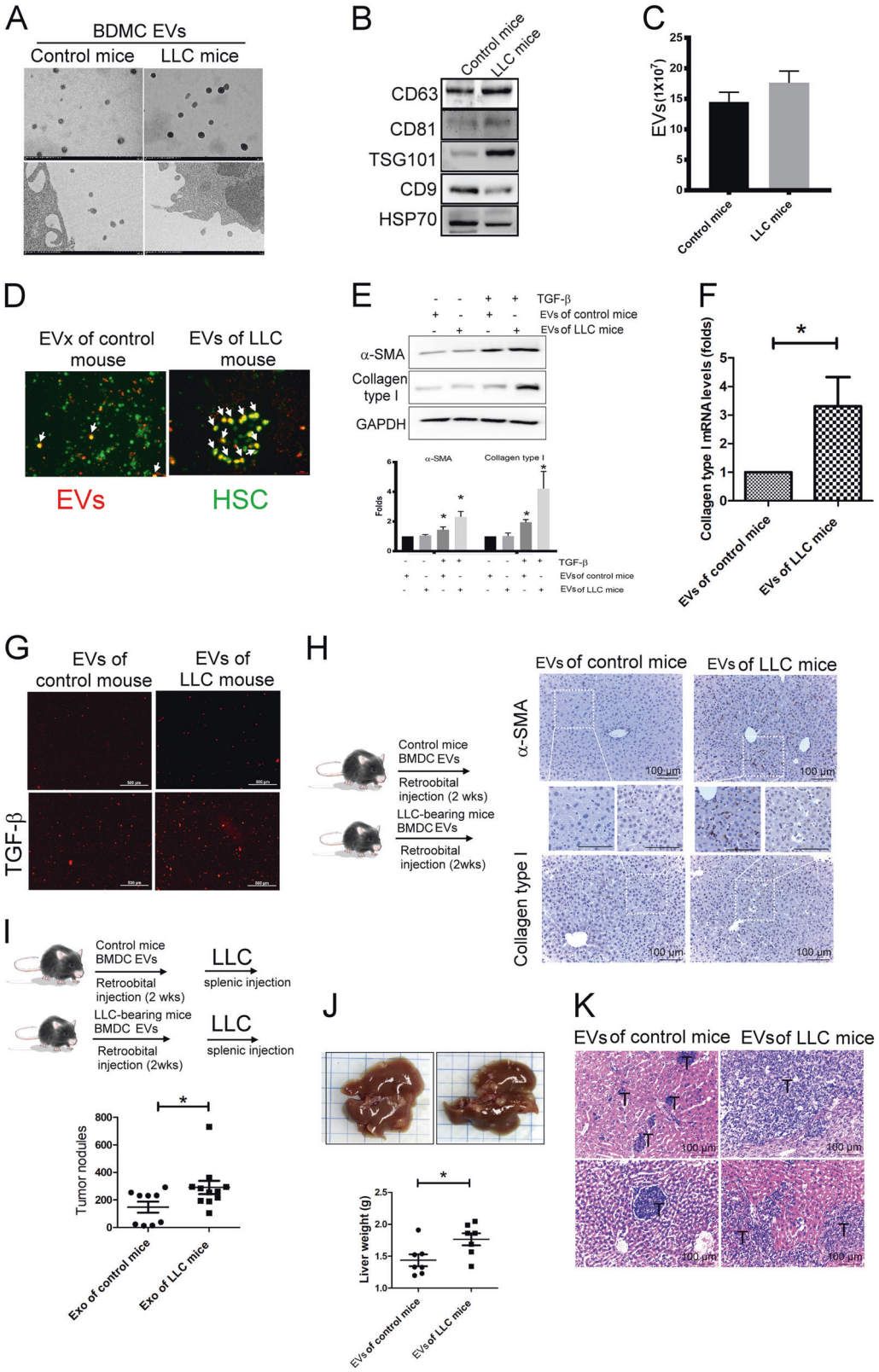

were significantly higher in lung cancer patients (Fig. 6a). LX2 cells were used to assess activation of EVs isolated from the serum of lung cancer patients. As shown in Fig. 6b, c, activation and collagen type I expression of LX2 cells were enhanced in the presence of EVs isolated from patients' sera. Sera presenting high levels of EVs miR-92

◀ **Fig. 2** BMDC-derived EVs contribute to the formation of liver PMN. The characteristics of EVs as determined by TEM (**a**), immunoblot analysis (**b**) and quantitated by FluoroCet analysis (**c**). LLC was implanted into mice by tail vein injection. After 21 days, the BMDCs were collected and EVs obtained from the supernatants of BMDC after 48 h incubation. **d** The uptake of BMDC-derived EVs by mHSC. DiI-labeled BMDC-derived EVs (produced by 1×10^6 BMDCs) were added to mHSCs (1×10^5) for 6 h. The arrowhead indicates HSC uptake BMDC-derived EVs. The effect of BMDC-derived EVs on mHSC activation (**e**) and collagen type I expression (**f**). mHSCs were treated with EVs isolated from BMDCs of normal or LLC-bearing mice. The expressions of α-SMA and collagen type I were assessed by immunoblot and qRT-PCR, respectively. **g** EVs isolated from BMDC of LLC-bearing mice increased the attachment of LLC on mHSC cells. **h** EVs isolated from BMDC of LLC-bearing mice increased HSC activation and collagen expression in the livers. liver metastasis of lung cancer in vivo. EVs isolated from BMDC of LLC-bearing mice increased liver metastasis, as presented by tumor nodules (**i**), liver weight (**j**), and H&E staining (**k**). Mice were pretreated with EVs isolated from BMDCs of control and LLC-bearing mice by retro-orbital injection (5 μg/mice) for 3 weeks, then LLC was implanted into mice via splenic injection. After 20 days, the livers of these mice were harvested and stained with H&E. All results are representative of at least three independent experiments and each value is the mean ± SEM of three determinations; $^*p < 0.05$, ns not significant. EV extracellular vesicle, TGF-β transforming growth factor beta

exhibited greater stimulatory effect of HSC activation in LX2 cells. Similarly, the promotive effect of sera on the upregulation of collagen type I in LX2 cells was positively correlated with miR-92a levels (Fig. 6d). Our results convincingly prove that high levels of circulating miR-92a effectively increase HSC activation among lung cancer patients.

Discussion

The liver is well known as the target organ for metastases of various tumors, including lung, breast, pancreatic, stomach, and colorectal cancers [20–22]. Pancreatic ductal adenocarcinomas secrete tissue factor to increase platelet activation and thrombus formation in liver PMN, which facilitates the arrest of disseminated cancer cells [23]. Metastasis-promoting bone-marrow-derived cells, such as macrophages, and Kupffer cells activate HSCs by granulin and TGF-β, which in turn induces the deposition of periostin and collagen in the liver [23, 24]. The occurrence of liver metastasis is a poor prognostic sign for patients [25]. In this study, we describe for the sequential steps of hepatic PMN formation by BMDCs-released EVs. Cancer alters the miRNAs expression of BMDCs, leading them to deliver EV miR-92a to HSC in the liver. Consequently, miR-92a potentiates HSC activation and ECM remodeling, which promotes the recruitment of gMDSC to the liver, providing an immunosuppressive microenvironment for liver metastasis (Fig. 6e).

BMDC-derived cells have been implicated in contributing to metastasis by fostering the formation of PMNs, which support cancer cell colonization and proliferation, thereby promoting tumor metastasis [26–28]. Vascular endothelial growth factor receptor 1^+ hematopoietic progenitor cells, $CD11b^+$ myeloid cells, and regulatory and suppressive immune cells have been identified as important mediators of cancer metastasis to the lungs or liver by secreting inflammatory cytokines, growth factors, and proangiogenic molecules [28–30]. Currently, attention is focusing on to how mobilized and recruited BMDCs contribute to the formation of existing pre-metastatic sites driven by cancer cells via local communication, but relatively little is known about whether they also orchestrate the formation of pre-metastatic sites before mobilization. In this study, we elucidate for the first time the influence of BMDC in the preparation of liver pre-metastatic niche formation by a distant interaction. Lung cancer cells change the gene profile of BMDC, which in turn increases HSC activation and collagen type I production. In addition, administration of BMDC secretome from LLC-bearing mice enhances liver metastasis in recipient mice; supporting BMDCs also contribute to the formation of liver pre-metastatic niche at a stage prior to mobilization and recruitment.

Extracellular vesicles-based communication *represents* an *important* mode for cancer-tumor microenvironment bidirectional cross-talk at both long and short distances [31]. Currently, *miRNAs have been* considered to be the major *components* of EVs, which are critically involved in nearly all aspects of oncology, such as tumorigenesis, proliferation, apoptosis, progression, and metastasis, as well as drug resistance, by targeting oncogenes or tumor suppressor genes [32–34]. Secretory miRNAs are considered to contribute to the remodeling of the tumor-surrounding environment and PMN [31–33]. Pancreatic ductal adenocarcinomas stimulate hepatic Kupffer cells then trigger a cascade, which primes the fibrotic liver microenvironment for future metastasis [9]. miR-122-enriched EVs released by breast cancer cells decrease glucose uptake in astrocytes and lung fibroblasts, thereby increasing breast cancer metastasis [32]. Rat adenocarcinoma-derived EVs contain high levels of miR-494 or miR-542-3p, which target cadherin-17 and enhances MMP-2 and -9 expression in pre-metastatic lung stroma cells [34]. In this study, we found that miR-92a potentiates HSC activation, which in turn expresses high levels of collagen type I, resulting in the enhancement of cancer cell attachment and gMDSC recruitment. In addition, blockade of miR-92a decreases BMDC-mediated HSC activation and collagen type I deposition in liver, resulting in decreased hepatic PMN formation induced by lung cancer. Most importantly, considering that circulating miR-92a levels are increased in the serum of lung cancer patients, and that these increased

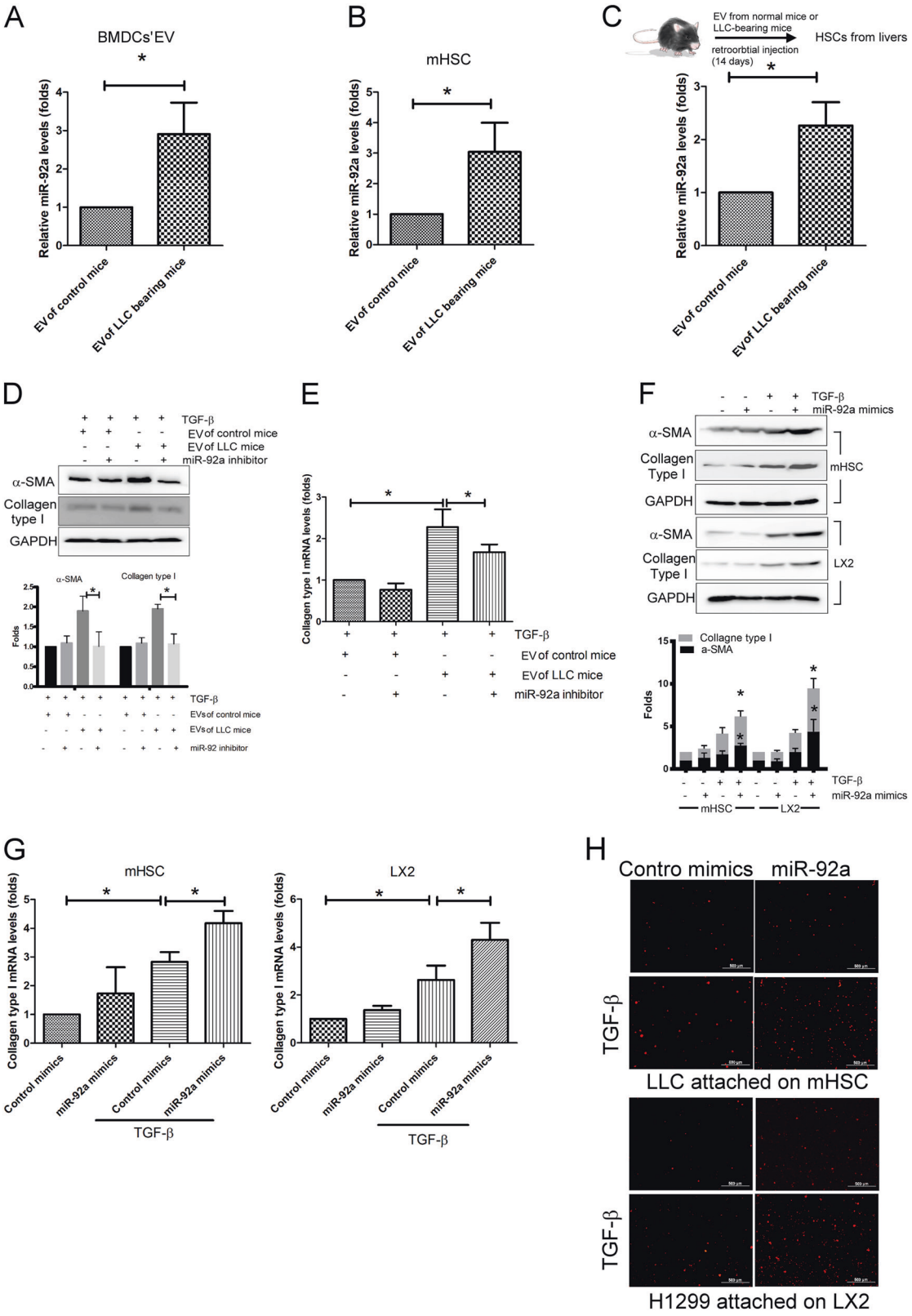

serum levels are positively associated with HSC activation and ECM remodeling, this suggests that EV miR-92a might be one of the key factors for liver pre-metastatic niche formation reinforced by BMDC.

◀ **Fig. 3** EV miR-92a-3p increased mHSC activation. **a** The levels of miR-92a-3p in EVs isolated from BMDCs of normal and LLC-bearing mice. LLC was implanted into mice by tail vein injection. After 21 days, the BMDCs were collected and the EVs were harvested after 48 h incubation. The expression of miR-92a-3p was assessed using qRT-PCR. **b** The level of miR-92a in mHSC which received BMDCs EVs. mHSCs (1×10^5 cells) were treated with EVs isolated from BMDCs (1×10^6 cells) of normal or LLC-bearing mice for 24 h. **c** The levels of miR-92a-3p in mHSC isolated from livers of normal and LLC-bearing mice. Mice were treated with EVs isolated from BMDCs of control and LLC-bearing mice by retro-orbital injection (5 μg/mice) for 2 weeks. HSC was isolated from the livers of mice and miR-92a levels was detected by qRT-PCR. miR-92a inhibitor prevented mHSC activation (**d**) and collagen type I expression (**e**) induced by EVs isolated from BMDCs of LLC-bearing mice. mHSCs were transfected either with control or miR-92a inhibitor for 24 h, then treated with EVs and TGF-β for 48 and 24 h, respectively. miR-92a mimics increased HSC activation (**f**), collagen type I expression (**g**), and lung cancer attachment (**h**). mHSC and LX2 cells were transfected with control or miR-92a mimics (100 nM) for 24 h, then treated with or without TGF-β for 24 h. The expressions of α-SMA and collagen type I were assessed by immunoblot and qRT-PCR, respectively. All results are representative of at least three independent experiments and each value is the mean ± SD of three determinations; $*p < 0.05$. HSC hepatic stellate cells, mHSC mouse HSC

Emerging evidence proves the role of TGF-β in the activation of HSCs during liver metastasis. High levels of TGF-β in lung cancer patients are associated with poor prognoses [35, 36]. SMAD7, an inhibitory SMAD protein, can compete with regulatory SMAD protein (R-SMAD) SMAD2/3 for binding to the TGF type I receptor and prevent their activation. SMAD7 also can disrupt TGF-β signaling by increasing TGF-β receptors' degradation and decreasing R-SMAD-DNA complex formation [37]. Overexpression of SMAD7 inhibits HSC transdifferentiation, resulting in reduced liver fibrosis in rats, whereas repression of SMAD7 increases HSC activation in liver fibrosis [38, 39]. Our study has confirmed that BMDC-derived miR-92a transferred via EVs effectively reduces SMAD7 expression and increases the phosphorylation of SMAD2 in recipient HSCs. BMDC-derived miR-92a directly targets the 3'UTR of SMAD7 in HSCs. HSC activation and collagen type I upregulation induced by miR-92a mimics is prevented by miR-92a inhibitor. Conversely, SMAD7 overexpression inhibits HSC activation and collagen type I deposition in miR-92a mimics-treated HSCs, providing additional evidence that miR-92a increases SMAD7 transcript degradation, resulting in HSC activation and cell matrix deposition

Taken together, our study reveals BMDCs contribute to formation of hepatic PMN, which primes HSC activation and increases ECM deposition to support cancer and gMDSC attachment. Our results reveal a new mechanism by which cancer cells alter BMDCs, which potentiate PMN formation via a previously undescribed EV miR-92a → SMAD7 regulatory pathway. Our study provides novel therapeutic options to inhibit liver metastasis by decreasing PMN formation prior to the spread of cancer, including the targeting of EV miR-92a and mechanisms promoting cancer colonization engaged by HSC activation.

Materials and methods

Cell culture

Human lung cancer H460 and mouse LLC cells were obtained from the American Type Culture Collection (ATCC). LX2 cells, which are immortalized human-derived HSCs, were obtained from the EMD Millipore (Billerica, MA). H460 cells were cultured in Roswell Park Memorial Institute (RPMI) 1640 supplemented with 10% fetal bovine serum (FBS) and 1% penicillin-streptomycin (Lonza, Walkersville, MD). LLC and LX2 cells were cultured in Dulbecco's Modified Eagle Medium (DMEM) with 10 and 2% FBS, respectively. H460 cells were authenticated by short tandem repeat analysis using the Geneprint 10 System Kit (B9510, Promega, Madison, WI, USA). All cell lines were tested for mycoplasma contamination using mycoplasma test kits (Mycoalert Mycoplasma Detection Kit) (Lonza) every 3 months.

The isolation of BMDC, HSC, MDSC, HPCs, and CD11b$^+$ cells

C57BL/6 J and nude mice mice were purchased from the National Laboratory Animal Center (*Taipei*, Taiwan). All animal experiments were performed in accordance with the Institutional Animal Care and Use Committee, and with the approval of the Animal Care and Use Committee of the School of Kaohsiung Medical University. Each mouse (male, 8-weeks-old, $n = 6$) was implanted with LLC (1×10^6/ C57BL/6 J mouse) or H460 (1×10^6/nude mice) via tail vein injection for 10 (for NGS analysis) or 21 days (for EVs collection). Mouse HSC of normal or LLC-bearing mice were isolated from normal and LLC-bearing mice by collagenase-pronase (Sigma–Aldrich, St. Louis, MO) perfusion and subsequent density centrifugation on Nycodenz gradients (Sigma–Aldrich), as described previously [20]. mHSCs were cultured in DMEM supplemented with 10% FBS and 1% penicillin-streptomycin (Lonza). Bone marrow cells were collected under sterile conditions with Hank's balanced salt solution from the medullary cavities of tibiae and femurs using a 25-gauge needle. The isolation of MDSC, HPC and CD11b$^+$ cells was carried out using a myeloid-derived suppressor cell isolation kit (Miltenyi Biotech, Germany), MojoSort™ Mouse Hematopoietic Progenitor Cell Isolation kit (BioLegend, San Diego, CA) and CD11b microbeads (Miltenyi Biotech), respectively.

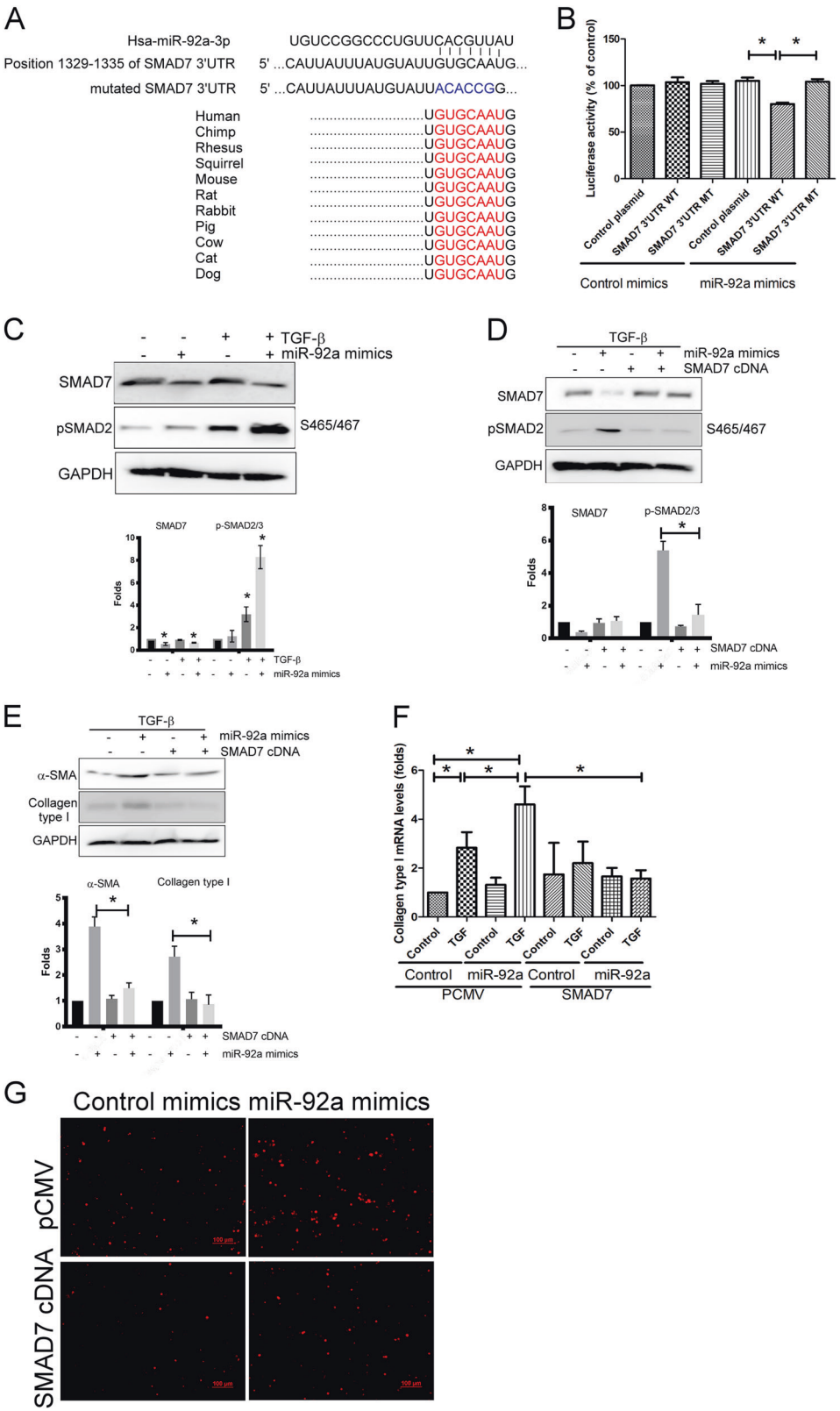

Fig. 4 SMAD7 is the target of EV miR-92a-3p. **a** Sequence alignment of the *SMAD7* 3AD7nce alignment of the ls, mHSC, **b** The binding capacity of miR-92a on the 3'UTR of SMAD7, as determined by report analysis. *SMAD7* 3'UTR firefly luciferase reporter vector and renilla luciferase control vector allowed simultaneous monitoring of miR-92a activity and transfection efficiency, respectively. **c** miR-92a mimics decreased the expression of SMAD7. LX2 cells were transfected with control or miR-92a mimics, then levels of various proteins were assessed by immunoblot after 48 h transfection. Overexpression of SMAD7 prevents miR-92a in the regulation of TGF-β signaling (**d**), HSC activation (**e**), collagen type I expression (**f**), and lung cancer attachment (**g**). SMAD7 overexpressing LX2 cells were transfected with transfected either with control or miR-92a mimics (100 nM) for 48 h. Protein levels were assessed by immunoblot. All results are representative of at least three independent experiments and each value is the mean ± SD of three determinations; $*p < 0.05$

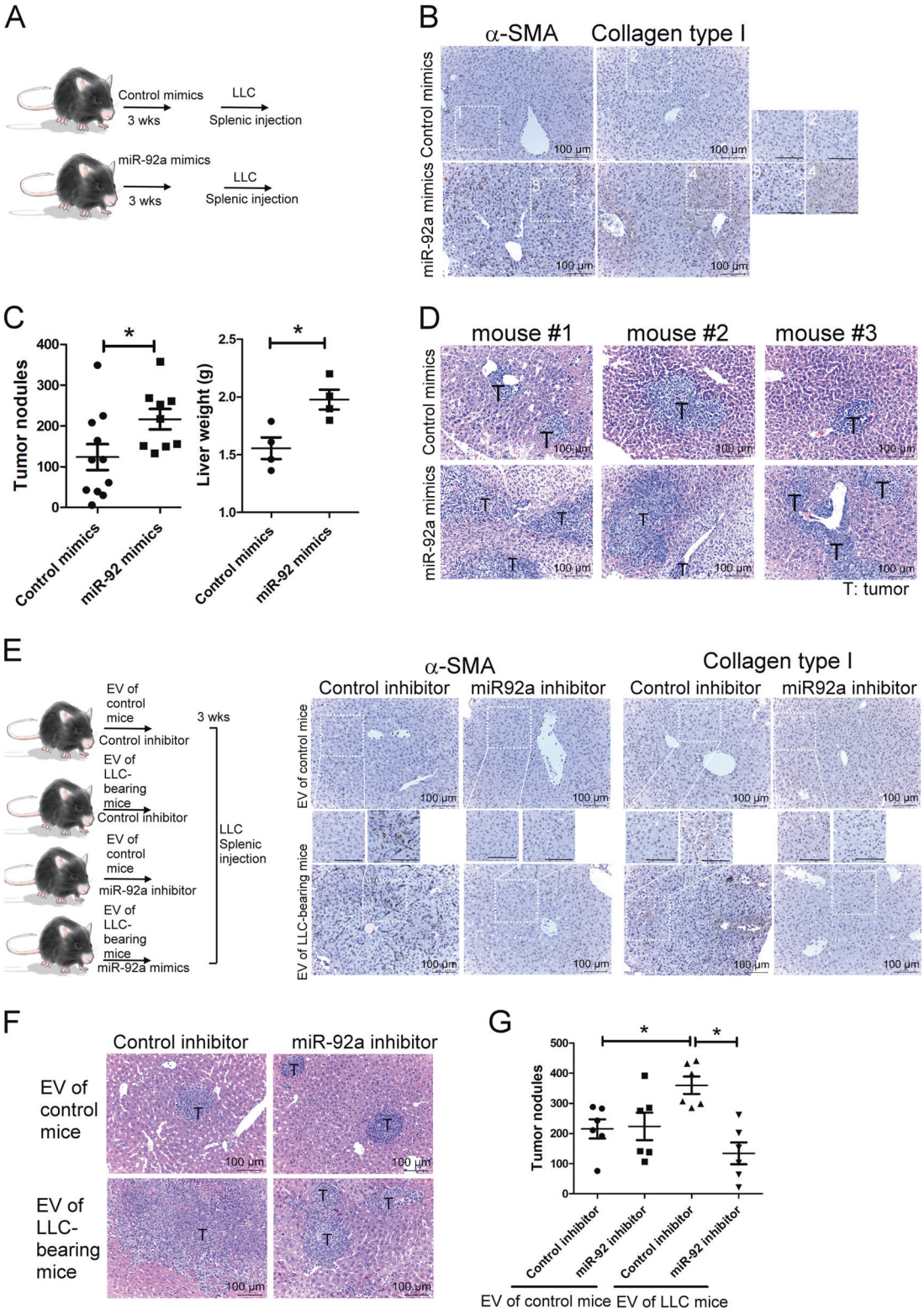

Fig. 5 miR-92a increased liver metastasis of lung cancer in vivo. **a** Scheme of animal model. **b** HSC activation and collagen type I expression in the livers of mice. Control or miR-92a mimics (5 μg/mouse) mixed with in vivo-*jetPEI* was delivered seven times retro-orbital injection prior to LLC implantation. mHSC activation was determined by α-SMA staining. **c** miR-92a increased liver metastasis. (**d**) H&E staining of liver tumor sections. miR-92a inhibitor decreased HSC activation and collagen type I expression in livers of mice **e**. miR-92a inhibitor decreased liver metastasis, as presented by H&E staining (**f**) and the numbers of tumor nodules in the livers (**g**). All results are representative of at least three independent experiments and each value is the mean ± SEM of three determinations; $^{*}p < 0.05$

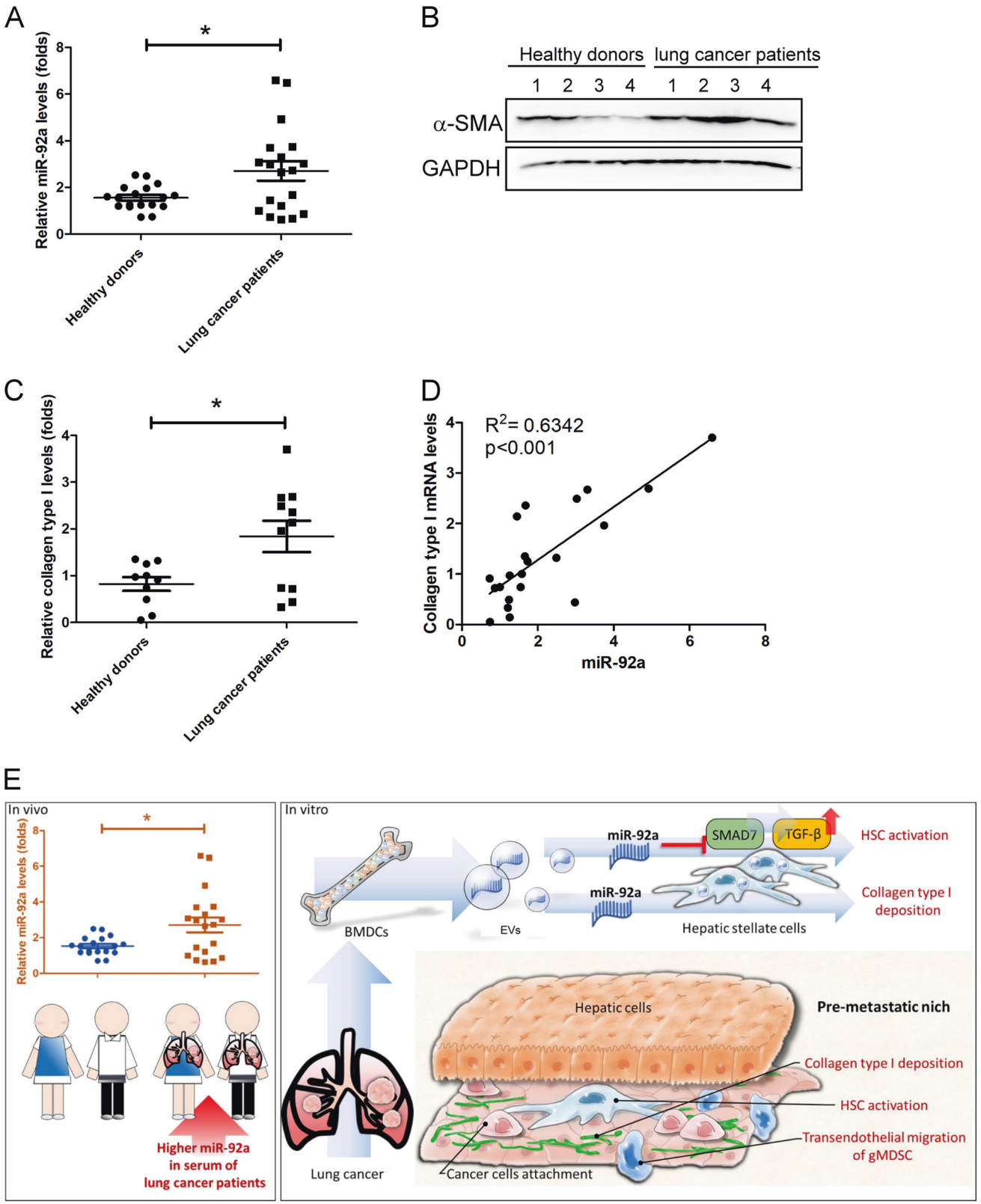
A
Relative miR-92a levels (folds)
Healthy donors
Lung cancer patients
B
Healthy donors
lung cancer patients
1 2 3 4 1 2 3 4
α-SMA
GAPDH
C
Relative collagen type I levels (folds)
Healthy donors
Lung cancer patients
D
R2= 0.6342
p<0.001
Collagen type I mRNA levels
miR-92a
E
In vivo
Relative miR-92a levels (folds)
Higher miR-92a in serum of lung cancer patients
In vitro
BMDCs
EVs
miR-92a
SMAD7
TGF-β
HSC activation
Collagen type I deposition
Hepatic stellate cells
Lung cancer
Hepatic cells
Pre-metastatic nich
Collagen type I deposition
HSC activation
Transendothelial migration of gMDSC
Cancer cells attachment

◀ **Fig. 6** Elevated circulating miR-92a in lung cancer patients. **a** The levels of EV miR-92a in healthy donors and lung cancer patients. EVs were isolated from the sera of healthy donors or lung cancer patients, and miR-92a levels assessed by qRT-PCR. EVs isolated from lung cancer patients' sera enhanced LX2 activation (**b**) and collagen type I expression (**c**). The correlation of miR-92a levels with the stimulatory effect in collagen type I expression (**d**). EVs were isolated from the sera of healthy donors or lung cancer patients, and miR-92a levels were assessed by RT-PCR. LX2 cells were treated with EVs (1 μg) isolated from sera of lung cancer patients or healthy donors. The expression of α-SMA and collagen type I was assessed by immunoblot and qRT-PCR, respectively. **e** Model for how BDMC-derived EVs increase the formation of liver PMN, which promotes lung cancer metastasis. All results are representative of at least three independent experiments and each value is the mean ± SEM of three determinations; $*p < 0.05$

Cell viability types were checked using trypan blue staining, and cell purity was checked using specific antibody staining and a flow cytometry.

Isolation of EVs from cell supernatants and patient sera

BMDCs were seeded at a density of 2×10^6 cells/100 mm dish and cultured in RPMI1640 containing 1% exosome-free serum (Life Technologies, Grand Island, NY) for 24 h. EVs derived from BMDCs were purified using total exosome isolation reagents (from cells) (Life Technologies, Grand Island, NY) after removing cell debris by differential centrifugation, following the manufacturer's guidelines. Quantitation of EVs of BMDCs was carried out by FluoroCet dye (*SBI* System Biosciences, CA, USA), which measures the activity of a known EV protein acetecylcholinesterase.

Sera were obtained from 19 lung cancer patients and 18 healthy donors admitted to the Division of Pulmonary and Critical Care Medicine at Kaohsiung Medical University Hospital (KMUH), Kaohsiung, Taiwan. The Institutional Review Board of KMUH approved the study's protocol, and all participants provided written informed consent in accordance with the Declaration of Helsinki. EVs derived from sera were purified by total exosome isolation reagents (for sera) (Life Technologies, Grand Island, NY) as described by the manufacturer. EVs protein content was quantified using bicinchoninic acid protein assay (Millipore).

RNA Isolation, *NGS* and Quantitative Real-time Polymerase Chain Reaction (qPCR)

Total RNA from the BMDCs and EVs was isolated using TRIzol and TRIzolLS Reagent (Life Technologies), respectively. The small RNA library construction and deep sequencing was conducted by the biotechnology company Welgene, based in Taipei, Taiwan. Samples were prepared using Illumina sample preparation kit according to the TruSeq Small RNA Sample Preparation Guide. The 3ruSeqe TruSeqwas conducted by the biotechnology company Welgene, basedwas followed by PCR amplification. The enriched cDNA constructs were size-fractionated and purified on a 6% polyacrylamide gel electrophoresis. Libraries were sequenced on an Illumina instrument (75SE cycle single read) and processed using the Illumina software.

cDNA was prepared using an oligo (dT) primer and reverse transcriptase (Takara, Shiga, Japan) following standard protocols. miRNAs isolated from EVs were reverse transcribed using the Mir-X™ miRNA First Strand Synthesis Kit (Clontec). RNA levels were determined using real-time analysis with SYBR Green on a StepOne-Plus machine (Applied Biosystems, Foster City, CA, United States). miRNAs isolated from various organs were reverse transcribed using the TaqMan™ Advanced miRNA cDNA Synthesis Kit, and miR-92a levels determined by TaqMan™ Advanced Master Mix (Thermo Fisher Scientific). The relative expressions of mRNA in cells were normalized to GAPDH. The expression of miR-92a in EVs isolated from BMDCs, serum or organs was normalized with spike-in control cel-miR-39 (Exiqon, Vedbaek, Denmark) and compared with a reference sample. The primers used are listed in sTable 2.

Fluorescent imaging of EVs uptake

EVs derived from BMDCs of normal and LLC-bearing mice were labeled with Dil dye (Life Technologies), and then incubated with mHSC for 6 h. After washing, mHSCs were stained with Calcein-AM (Life Technologies) for 30 min, and photographed using a Nikon inverted fluorescence microscope (Eclipse TE200 microscope).

Analysis of transendothelial migration and cell adherence

mHSCs were treated with EVs isolated from BMDCs of normal and LLC-bearing mice, then treated with or without TGF-β (2.5 ng/ml) for 24 h. C166 cells were seeded onto inserts with polyester membranes of 1 μm pore size (EMD Millipore) for 2 days. PKH26-labeled MDSCs were seeded onto C166 coated inserts, which were suspended in the wells of mHSC-seeded plates for 24 h. Migratory MDSCs were made visible using a fluorescence microscope.

LX2 or mHSCs were transfected with control or miR-92a mimics for 24 h, then treated with or without TGF-β (2.5 ng/ml) for 24 h. PKH26-labeled H1299 or LLC were seeded onto LX2 cells or mHSC monolayers for 30 min, respectively. Alternatively, mHSCs were treated with EVs isolated

from BMDCs of normal and LLC-bearing mice, then treated with or without TGF-β (2.5 ng/ml) for 24 h. PKH26-labeled H1299 or LLC were seed onto LX2 cells or mHSC monolayers for 30 min, respectively. After washing with PBS, adherence H1299 or LLC was made visible using a fluorescence microscope.

Immunoblot

All samples were lysed by RIPA solution and the extracted proteins mixed immediately with equal volumes of SDS-loading buffer then boiled for 5 min. Equal volumes of total proteins were electrophoresed onto an 8–10% SDS-polyacrylamide gels and transferred onto PVDF membranes. After blocking, the membranes were blotted with primary antibodies and then HRP-conjugated secondary antibodies. The membrane signals were developed using the enhanced cheminulescence light (ECL) detecting kit (EMD Millipore). Antibodies against CD9, CD63, CD81, and HSP70 were obtained from SBI System Biosciences (Mountain View, CA, USA; Catalog #EXOAB-KIT-1). Antibodies against pSMAD2 (Catalog #3108), and GAPDH (Catalog #5174) were obtained from Cell Signaling Technology (Beverly, MA, USA). The antibodies against SMAD7 (Catalog # ST1625) were obtained from EMD Millipore. Anti-α-SMA antibody (Catalog # A2547) was obtained from Sigma. Anti-collagen type I antibody (Catalog # ab34710) was obtained from Abcam. The quantitation result of the Immunoblot was performed using AlphaImager software (Alpha Innotech, San Leandro, CA, USA).

SMAD7 3′UTR reporter assay, SMAD7 overexpression and miR-92a mimic transfection

LX2 cells were maintained at 50–60% confluence and co-transfected with control, SMAD7 3and miR-92a mimic transfeOrigene, Rockville, MD)/Renilla luciferase plasmid and control miRNA or miR-92a mimics using DharmaFECT duo transfection reagent (DHARMACON, Lafayette, CO) according to the manufacturer's protocol. After 48 h of incubation, luciferase activity was assayed using Steady–Glo Luciferase Assay System (Promega, Madison, WI). Renilla luciferase activity was used as a control for transfection efficiency. Overexpression of SMAD7 was achieved by transfecting SMAD7 cDNA (Origene Technologies, Rockville, MD, USA) via Lipofectamine 2000 transfect reagent (Thermo Fisher Scientific), and a stable cell line was established by G418 screening. LX2 cells were transfected with scrambled control (Negative Control) or miR-92a mimic, (DHARMACON), by using *Lipofectamine RNAiMAX* Transfection Reagent (Thermo Fisher Scientific, Waltham, MA, USA).

In vivo delivery of BMDC-derived EVs and miR-92a

Each mouse (male, 8-week-old C57BL/6, $n = 6–8$) received bone marrow cell-derived EVs isolated from normal or LLC-bearing mice through retro-orbital injections (three times/week, 5 μg/mice/time) for 3 weeks. Alternatively, mice received 5 μg of control or miR-92a mimics mixed with 1.6 μL in vivo-JetPEI transfection reagent in 50 μL normal saline, which was delivered nine times by retro-orbital injection at 3-day intervals. Mice were injected intrasplenically with 1×10^6 LLC and tumor development was followed for 21 days following the first injection. Mice were euthanized and the tumor nodules of livers counted. Blood samples were collected via cardiac puncture and blood biochemical assay was conducted by National Laboratory Animal Center (Taipei, Taiwan). Levels of miR-92a and cytokines of organs were assessed by qRT-PCR. Organs were embedded in paraffin, sectioned, and stained with hematoxylin and eosin (H&E) for histological examination using standard techniques. The expressions of α-SMA and collagen type I were demonstrated using mouse monoclonal anti-α-SMA (dilution 1:200) and anti-collagen type I (dilution 1:100, Abcam Ltd. Cambridge, UK) antibodies, respectively. All of the sectioned tissues were counterstained with hematoxylin.

Statistical analysis

All data were analyzed using GraphPad Prism 5 (GraphPad Software, La Jolla, CA), and differences between the means for each condition were evaluated by a one-way ANOVA followed by a Tukey post-hoc test.

Acknowledgements The authors gratefully acknowledge the support of research grants from the Ministry of Science and Technology (MOST 107-2320-B-037-011-MY3; MOST 104-2314-B-037-053-MY4), the Kaohsiung Medical University Hospital (KMUHS10701; KMUHS10712), the Kaohsiung Medical University (KMU-DK108003; KMU-DK108008; KMU-TC108A04), and the E-DA Cancer Hospital Research Foundation (EDCHI107001). The authors thank the Center for Research Resources and Development of Kaohsiung Medical University.

Compliance with ethical standards

Conflict of interest The authors declare that they have no conflict of interest.

Publisher's note Springer Nature remains neutral with regard to jurisdictional claims in published maps and institutional affiliations.

References

1. Siegel RL, Miller KD, Jemal A. Cancer statistics, 2018. CA Cancer J Clin. 2018;68:7–30.

2. Jiang T, Cheng R, Zhang G, Su C, Zhao C, Li X, et al. Characterization of Liver Metastasis and Its Effect on Targeted Therapy in EGFR-mutant NSCLC: A Multicenter Study. Clin Lung Cancer. 2017;18:631–9.e2.
3. Tsao AS, Scagliotti GV, Bunn PA, Jr, Carbone DP, Warren GW, Bai C. et al. Scientific Advances in Lung Cancer. J Thorac Oncol. 2016;11:613–38.
4. Liu Y, Gu Y, Han Y, Zhang Q, Jiang Z, Zhang X, et al. Tumor Exosomal RNAs Promote Lung Pre-metastatic Niche Formation by Activating Alveolar Epithelial TLR3 to Recruit Neutrophils. Cancer Cell. 2016;30:243–56.
5. Peinado H, Zhang H, Matei IR, Costa-Silva B, Hoshino A, Rodrigues G, et al. Pre-metastatic niches: organ-specific homes for metastases. Nat Rev Cancer. 2017;17:302–17.
6. Aguado BA, Bushnell GG, Rao SS, Jeruss JS, Shea LD. Engineering the pre-metastatic niche. Nat Biomed Eng. 2017;1:0077.
7. Chang YP, Chen YM, Lai CH, Lin CY, Fang WF, Huang CH, et al. The impact of de novo liver metastasis on clinical outcome in patients with advanced non-small-cell lung cancer. PLoS ONE. 2017;12:e0178676.
8. Kang N, Gores GJ, Shah VH. Hepatic stellate cells: partners in crime for liver metastases? Hepatology. 2011;54:707–13.
9. Costa-Silva B, Aiello NM, Ocean AJ, Singh S, Zhang H, Thakur BK, et al. Pancreatic cancer exosomes initiate pre-metastatic niche formation in the liver. Nat Cell Biol. 2015;17:816–26.
10. Barbazán J, Alonso-Alconada L, Elkhatib N, Geraldo S, Gurchenkov V, Glentis A, et al. Liver metastasis is facilitated by the adherence of circulating tumor cells to vascular fibronectin deposits. Cancer Res. 2017;77:3431–41.
11. Tsuchida T, Friedman SL. Mechanisms of hepatic stellate cell activation. Nat Rev Gastroenterol Hepatol. 2017;14:397–411.
12. Redig AJ, McAllister SS. Breast cancer as a systemic disease: a view of metastasis. J Intern Med. 2013;274:113–26.
13. Kim KW, Lee SJ, Kim WY, Seo JH, Lee HY. How can we treat cancer disease not cancer cells? Cancer Res Treat. 2017;49:1–9.
14. Lin LY, Du LM, Cao K, Huang Y, Yu PF, Zhang LY, et al. Tumour cell-derived exosomes endow mesenchymal stromal cells with tumour-promotion capabilities. Oncogene. 2016;35:6038–42.
15. Engblom C, Pfirschke C, Zilionis R, Da Silva Martins J, Bos SA, Courties G, et al. Osteoblasts remotely supply lung tumors with cancer-promoting $SiglecF_{high}$ neutrophils. Science. 2017;358:eaal5081.
16. Adler BJ, Kaushansky K, Rubin CT. Obesity-driven disruption of haematopoiesis and the bone marrow niche. Nat Rev Endocrinol. 2014;10:737–48.
17. Taylor D, Wilkison M, Voyich J, Meissner N. Prevention of bone marrow cell apoptosis and regulation of hematopoiesis by type I IFNs during systemic responses to pneumocystis lung infection. J Immunol. 2011;186:5956–67.
18. Deng Z, Rong Y, Teng Y, Zhuang X, Samykutty A, Mu J, et al. Exosomes miR-126a released from MDSC induced by DOX treatment promotes lung metastasis. Oncogene. 2017;36:639–51.
19. Zhang L, Zhang S, Yao J, Lowery FJ, Zhang Q, Huang WC, et al. Microenvironment-induced PTEN loss by exosomal microRNA primes brain metastasis outgrowth. Nature. 2015;527:100–4.
20. Mederacke I, Hsu CC, Troeger JS, Huebener P, Mu X, Dapito DH, et al. Fate tracing reveals hepatic stellate cells as dominant contributors to liver fibrosis independent of its aetiology. Nat Commun. 2013;4:2823.
21. Hashimoto M, Kobayashi T, Tashiro H, Arihiro K, Kikuchi A, Ohdan H. h-Prune is associated with poor prognosis and epithelial-mesenchymal transition in patients with colorectal liver metastases. Int J Cancer. 2016;139:812–23.
22. Burnier JV, Wang N, Michel RP, Hassanain M, Li S, Lu Y, et al. Type IV collagen-initiated signals provide survival and growth cues required for liver metastasis. Oncogene. 2011;30:3766–83.
23. Houg DS, Bijlsma MF. The hepatic pre-metastatic niche in pancreatic ductal adenocarcinoma. Mol Cancer. 2018;17:95.
24. Nielsen SR, Quaranta V, Linford A, Emeagi P, Rainer C, Santos A, et al. Macrophage-secreted granulin supports pancreatic cancer metastasis by inducing liver fibrosis. Nat Cell Biol. 2016;18:549–60.
25. Ren Y, Dai C, Zheng H, Zhou F, She Y, Jiang G, et al. Prognostic effect of liver metastasis in lung cancer patients with distant metastasis. Oncotarget. 2016;7:53245–53.
26. Hara T, Murakami Y, Seiki M, Sakamoto T. Mint3 in bone marrow-derived cells promotes lung metastasis in breast cancer model mice. Biochem Biophys Res Commun. 2017;490:688–92.
27. Xu WW, Li B, Guan XY, Chung SK, Wang Y, Yip YL, et al. Cancer cell-secreted IGF2 instigates fibroblasts and bone marrow-derived vascular progenitor cells to promote cancer progression. Nat Commun. 2017;8:14399.
28. Kaplan RN, Riba RD, Zacharoulis S, Bramley AH, Vincent L, Costa C, et al. VEGFR1-positive haematopoietic bone marrow progenitors initiate the pre-metastatic niche. Nature. 2005;438:820–7.
29. Liu Y, Cao X. Characteristics and significance of the pre-metastatic niche. Cancer Cell. 2016;30:668–81.
30. Brodt P. Role of the microenvironment in liver metastasis: from pre- to prometastatic niches. Clin Cancer Res. 2016;22:5971–82.
31. Grange C, Tapparo M, Collino F, Vitillo L, Damasco C, Deregibus MC, et al. Microvesicles released from human renal cancer stem cells stimulate angiogenesis and formation of lung pre-metastatic niche. Cancer Res. 2011;71:5346–56.
32. Fong MY, Zhou W, Liu L, Alontaga AY, Chandra M, Ashby J, et al. Breast-cancer-secreted miR-122 reprograms glucose metabolism in premetastatic niche to promote metastasis. Nat Cell Biol. 2015;17:183–94.
33. Xu R, Rai A, Chen M, Suwakulsiri W, Greening DW, Simpson RJ. Extracellular vesicles in cancer—implications for future improvements in cancer care. Nat Rev Clin Oncol. 2018;15:617–38.
34. Rana S, Malinowska K, Zöller M. Exosomal tumor microRNA modulates premetastatic organ cells. Neoplasia. 2013;15:281–95.
35. Huang AL, Liu SG, Qi WJ, Zhao YF, Li YM, Lei B, et al. TGF-β1 protein expression in non-small cell lung cancers is correlated with prognosis. Asian Pac J Cancer Prev. 2014;15:8143–7.
36. Coulouarn C, Factor VM, Thorgeirsson SS. Transforming growth factor-beta gene expression signature in mouse hepatocytes predicts clinical outcome in human cancer. Hepatology. 2008;47:2059–67.
37. ten Dijke P, Hill CS. New insights into TGF-beta-Smad signalling. Trends Biochem Sci. 2004;29:265–73.
38. Bian EB, Huang C, Wang H, Chen XX, Zhang L, Lv XW, et al. Repression of Smad7 mediated by DNMT1 determines hepatic stellate cell activation and liver fibrosis in rats. Toxicol Lett. 2014;224:175–85.
39. Dooley S, Hamzavi J, Breitkopf K, Wiercinska E, Said HM, Lorenzen J, et al. Smad7 prevents activation of hepatic stellate cells and liver fibrosis in rats. Gastroenterology. 2003;125:178–91.